Triple-jet production at large transverse momentum

B. L. Combridge*
Department of Applied Mathematics and Theoretical Physics, University of Cambridge, Cambridge, England
(Received 3 August 1976)

Aspects of large-p_T multiple-jet production in hadronic collisions are discussed. The possible magnitude and importance of such processes are investigated by making a detailed calculation of the triple-jet cross section in the quark-fusion model. The essential parameters of the model, including an over-all normalization, are known from fits to data of the (two-jet) quark-fusion model. Predictions for the two-pion invariant cross-section are given for various configurations and charge combinations of the pions. Many of these results are experimentally accessible, although they are often comparable with or exceeded by the results of a naive independent-production calculation. The total contribution of the triple-jet process to the large-p_T single-particle yield may not be negligible in the model.

I. INTRODUCTION

In parton-model descriptions of large-p_T inclusive processes, in which two jets with equal and opposite large transverse momenta are produced by a single hard scattering of hadronic constituents, the large-p_T particles in each event are approximately coplanar with the beam. This need not be so if more than two jets are produced in the hard-scattering subprocess. Such noncoplanar processes are interesting as tests of various theoretical ideas, as indicated below.

The term "jet" will be used here to denote collectively final-state systems of one or more particles in which the particles have limited momenta (typically 300 MeV/c) transverse to the jet axis (the direction of the total momentum of the system), but possibly widely varying momenta along this axis. We shall assume that the overall invariant mass of a jet is small compared with p_T, $\sqrt{s}$.

Present data on high-energy inclusive hadronic processes at large transverse momentum can be well described in terms of the production of two jets with equal and opposite large p_T.[1]

These jets are not necessarily identified with the quark jets of deep-inelastic processes or e^+e^- annihilation, and they need not have the same properties. For example, in the model described in Sec. II, the nature of the production mechanism ensures that the jets have physical quantum numbers *ab initio* and are thus immediately available as final states.

In parton models the usual production mechanism for the jets is a single hard scattering of two constituents from the initial-state hadrons.[2,3] Dimensional counting[4,5] implies that, for large s and fixed t/s, this subprocess is described by

$$\frac{d\sigma}{dt} \simeq s^{-N} f(t/s) \ , \tag{1.1}$$

where $(N+2)$ is the minimum total number of elementary fields (e.g., quarks) involved in the hard scattering. This gives the single-particle invariant cross section[5]

$$E\frac{d\sigma}{d^3p} \simeq s^{-N} F(x_T, \theta) \tag{1.2}$$

at large s, fixed $x_T = 2p_T/\sqrt{s}$ and center-of-mass scattering angle θ (assuming that the momentum distributions describing the particle content of the jets are scale-free at large jet momentum; i.e., they depend only on the ratio of the particle and jet momenta).

The scaling form (1.2) is a good description of the single-particle data, although the value of the power N appears to have some dependence on particle type.[6-8] This may reflect the presence of several hard-scattering mechanisms which dominate for different detected particles.[2,3] $N=4$ fits meson data[8] throughout the CERN ISR experimental range $23 \lesssim \sqrt{s} \lesssim 62$ GeV, $0.1 \lesssim x_T \lesssim 0.35$. In the following sections we restrict our considerations to this kinematic region and assume that the dominant mechanism giving this behavior for mesons is the quark-fusion process described in Sec. II. We shall not discuss a mechanism for baryon production, although there is, for example, a significant proton component at large p_T.

For a hard-scattering process in which the two constituents of the incoming hadrons (q_1, q_2) give rise to m jets $(q_3, \ldots, q_{m+2})$, the dimensional counting generalization of (1.2) for the $(m-1)$-particle cross section is[5]

$$E_3 \cdots E_{m+1} \frac{d\sigma}{d^3q_3 \cdots d^3q_{m+1}} \simeq s^{-N} H_1\left(\frac{q_i \cdot q_j}{s}\right) \tag{1.3}$$

as s becomes large together with the $q_i \cdot q_j$ $(i \neq j)$. Again $(N+2)$ is the minimum number of elementary fields associated with the hard scattering. The contribution of this process to the large-p_T single-particle cross section, *from a fixed region of* $q_i \cdot q_j/s$ *space*, scales as

$$E\frac{d\sigma}{d^3p} \simeq s^{-N+m-2}H_2(x_T,\theta)\ . \tag{1.4}$$

Provided that the function H_1 in (1.3) is not too singular as the $q_i\cdot q_j/s \to 0$, then the above qualification can be dropped and (1.4) holds generally for this process.[21] In this case, the two-jet mechanism is necessarily the dominant contribution to the single-particle cross section for s sufficiently large (x_T fixed), although multiple-jet mechanisms may still contribute significantly at intermediate energies.

The major relevance of such considerations for present experiments is that in a two-jet process all the large-p_T particles are roughly coplanar with the beams because of the limited transverse momentum of the initial-state partons. However, a multiple-jet mechanism can give rise to large-p_T particles with azimuthal separation ϕ away from 0° and 180°. Hence, with two detectors having, for example, $\phi = 90°$, such contributions, if they exist, can be studied separately from the two-jet processes which are expected to dominate the $\phi \simeq 0°$ and 180° angular regions.

Experimental data from this largely unexplored region will be an important test of current ideas on large-p_T events and may help to discriminate between the various parton and nonparton models. In the above framework, important questions are: Do the cross sections scale? If so, how? Is this compatible with dimensional counting? How much of the single-particle cross section at large p_T comes from multiple-jet events?

A particular point of interest is whether the cross sections for these processes are too small to be observed. Some of the values predicted by the three-jet model discussed below would appear to be accessible experimentally.

In the remainder of this paper we present a particular model of a three-jet process and give quantitative predictions of the invariant cross section for the production of two large-p_T pions. For present purposes we shall assume that the production of four or more jets gives only a small contribution to this process.

The model used is a straightforward generalization of a two-jet quark-fusion approach which has been reasonably successful in describing CERN ISR data on large-p_T mesons and, recently, large-p_T direct photons. The parameters of the model are fixed or constrained by the earlier fits to data. The resulting predictions for the three-jet process are determined to within an order of magnitude, with much of the uncertainty residing in the absolute normalization rather than the shapes or relative magnitudes of the cross sections. Some remarks on the model dependence of our results are given at the end of Sec. IV.

The quantitative predictions will be made for the CERN ISR energy point $\sqrt{s} = 52.7$ GeV, and for values of p_T similar to those used in present large-p_T correlation experiments at the CERN Split-Field Magnet. Results at other energies (higher, but not too much lower because of our small x_T values) can be obtained by a simple scaling.

The organization of this paper is as follows. Section II gives a brief description of the two-jet quark-fusion model and its comparison with experiment. Section III describes the natural extension of the model to triple-jet production, and obtains an expression for the two-meson invariant cross section. Section IV gives quantitative predictions of the two-pion cross section for various values of ϕ, transverse momenta, rapidities, and charge combinations of the two pions. Section V discusses further some of the points which have arisen.

Numerical results of the calculations described in Secs. III and IV are displayed in Tables II and III and in Figs. 6, 7 and 8. For comparison, Table IV gives results of a simple independent-production calculation for the two-pion cross section. From a parton-model standpoint, the intuitive physical interpretation associated with this approach would seem to be double scattering in which two pairs of jets are independently produced. However, it is not clear that such a contribution, at least as estimated by (4.5), is actually present.

For example, a detailed calculation of double scattering in the quark-fusion model is more complex and is dependent on extra assumptions. Perhaps we should regard Table IV as just a useful yardstick with which to compare the three-jet predictions.

II. QUARK-FUSION MODEL FOR LARGE-p_T MESON PRODUCTION

The model described below is essentially that due to Landshoff and Polkinghorne.[9] The main difference lies in the specific incorporation of a jet structure. This modification has also been described elsewhere.[10,11]

The hard-scattering subprocess is taken to be

$$q + \bar{q} \to \text{two jets}, \tag{2.1}$$

where the quarks are not colored and the two jets have meson quantum numbers. From (1.2), the single-particle inclusive cross section has the form

$$E\frac{d\sigma}{d^3p} \simeq s^{-4}F(x_T,\theta)\ , \tag{2.2}$$

which, as noted in Sec. I, is a reasonable descrip-

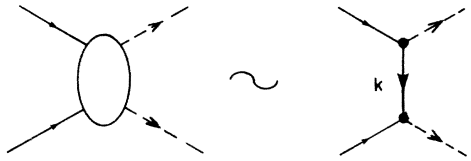

FIG. 1. Single-quark exchange approximation for the high-energy fixed-angle scattering $q+\bar{q}\to$ two jets (with meson quantum numbers).

tion of data in the ISR range.

Taking colored quarks in (2.1) and keeping the jets physical (i.e., uncolored) multiplies the function F in (2.2) by $\frac{1}{3}$. In order to preserve the two-jet fit to the single-particle data, certain vertex constants C_M, $C_{\rm jet}$ defined below must then be increased by a factor $(3)^{1/4}$. This would have the consequence that the quantitative predictions of Sec. IV for three-jet processes are multiplied by an overall net factor of $\sqrt{3}$.

To obtain an explicit form for the function F in (2.2) requires knowledge of the quark momentum distributions of the initial-state hadrons, a model for the hard-scattering amplitude, and information on the particle content of the jets.

The first of these can be derived from an analysis of the individual quark contributions to the deep-inelastic structure function:

$$\nu W_2(\omega)=\sum_{\substack{z=\mathfrak{G},\mathfrak{N},\lambda\\ \bar{\mathfrak{G}},\bar{\mathfrak{N}},\bar{\lambda}}} e_z{}^2F_2^z(\omega)\ . \tag{2.3}$$

The function $\omega F_2^z(\omega)$ may be regarded as the probability density for finding a quark of type z, with fractional momentum ω^{-1}, in the incident hadron.

The hard-scattering amplitude is assumed to be dominated by single-quark exchange (Fig. 1). The exchanged quark has large mass squared k^2. The form of its couplings to the jets is suggested by a Bethe-Salpeter equation approach to the pseudoscalar-meson vertex (see Ref. 12). This gives $C_M\gamma_5(-k^2)^{-\gamma}$, where C_M,γ are constants. Accordingly, the jet vertex will be assumed to have the effective form $C_{\rm jet}(-k^2)^{-1/2}$. [$\gamma=\frac{1}{2}$ is the value required for Fig. 1 to satisfy the dimensional counting result of (1.1). Also the γ-matrix structure of the vertices is taken to be simple; for many results this gives little difference anyway.] $C_{\rm jet}$ is a constant which may be regarded as given by

$$|C_{\rm jet}|^2=\sum_\alpha |C_\alpha|^2\ ,$$

where $C_\alpha(-k^2)^{-1/2}$ is the coupling for one of the final substates α that are collectively denoted by the term jet.

The jet is taken to consist of nonet final states with U(3)-symmetric couplings to the quarks. This does not give any significant quantitative difference from the SU(3) case, but simplifies the calculation by causing the contribution from interfering amplitudes to vanish identically in almost all cases.

The one remaining ingredient is a knowledge of the momentum distributions of particles in the jet. A recent analysis of large-p_T correlations in a general two-jet picture[13] indicates the presence of a single-particle mode of the jet, which, although small (a few percent of all jet final states), can, however, dominate the large-p_T triggers in single-particle inclusive experiments. This surprising fact arises from the large bias induced by the trigger. Since cross sections fall rapidly with transverse momentum, and a multiparticle jet generally has much larger p_T than its constituents, the single-particle mode of the jet is greatly enhanced.

Accordingly we make the simplifying assumption that the hard scattering in single-meson inclusive experiments at large p_T is (Fig. 2)

$$q+\bar{q}\to \text{meson (trigger)} + \text{jet (meson quantum numbers)}\ . \tag{2.4}$$

In all essential details, the calculation of the single-particle invariant cross section is as in Ref. 9 and gives

$$E\frac{d\sigma}{d^3p}\simeq\frac{C_M{}^2C_{\rm jet}{}^2}{32\pi^2p_T{}^8}\int_0^1 d\alpha_1 d\alpha_2\delta(\alpha_1+\alpha_2-1)\alpha_1{}^4 \times F^y_{2,H}\left(\frac{2\alpha_1}{x_T\cot\frac{1}{2}\theta}\right)F^z_{2,H'}\left(\frac{2\alpha_2}{x_T\tan\frac{1}{2}\theta}\right) + (\theta\to\pi-\theta,\quad H\leftrightarrow H') \tag{2.5}$$

summed over all contributing $q\bar{q}$ pairs (y,z). Note that (2.5) has the form of (2.2) as required. The two terms in (2.5) are the independent contributions of the two diagrams of Fig. 2. It turns out that their interference terms cancel exactly for SU(3) octet single-meson triggers if the antiquark distributions of H,H' are SU(3)-symmetric. The proton structure functions used in Ref. 9, and to be used here in Sec. IV, have this property. Explicitly they are

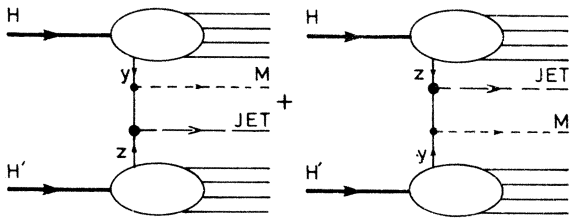

FIG. 2. (Two-jet) quark-fusion diagrams for $H+H'\to M+X$ at large p_T.

$$F_2^{\mathcal{P}}(\omega) = 2R + D, \quad F_2^{\mathfrak{N}}(\omega) = R + D,$$
$$F_2^{z}(\omega) = D, \quad z = \lambda, \bar{\mathcal{P}}, \bar{\mathfrak{N}}, \bar{\lambda} \tag{2.6}$$

where

$$R(\omega) = \frac{15}{16}\left(1 - \frac{1}{\omega}\right)^2 \omega^{-1/2},$$

$$D(\omega) = \frac{1}{10}\left(1 - \frac{2}{\omega}\right)\theta(\omega - 2).$$

The single-particle cross sections calculated from (2.5) and (2.6) agree reasonably well with ISR pp data. A fit to the large-p_T data of Ref. 8 for π^0 production and Ref. 6 for π^+, π^- gives the value $(C_M C_{\text{jet}})^{1/2} = 14$ GeV.

In the original model of Landshoff and Polkinghorne,[9] the basic process is $q + \bar{q} \to$ two pseudoscalar octet mesons. This leads to (2.5) with $C_M^2 C_{\text{jet}}^2$ replaced by C_M^4 (and so $C_M = 14$ GeV to fit data). There are also nonvanishing contributions from cross terms. However, there are no significant differences between this model and the present picture for the prediction of single-particle cross sections in pp interactions. In particular, both models give similar results for large-p_T particle ratios which agree well with ISR data[6] [except that the predicted K/π ratios are typically too high by a factor of 2 because of the assumption of exact SU(3)].

The introduction of a jet structure in the present model accommodates the increasing experimental evidence for jet production. There are also two other important direct consequences of this modification.

One is that a prediction,[14] that

$$\frac{\pi p \to \pi + X}{pp \to \pi + X} \gg 1 \text{ at large } p_T,$$

is substantially revised[10] and is in better agreement with data.[15] The other is that the cross sections predicted by Escobar for the production of large-p_T direct photons (by the mechanism of Fig. 3) are increased[11] relative to an earlier calculation[16] and are now compatible with recent ISR data.[17]

The parameter $\lambda = C_M^2/C_{\text{jet}}^2$, which is the probability that a freely produced jet consists of just a single particle, is not as yet well determined by the data. Consideration of the correlation, meson beam, and direct photon data suggest that λ is about 1–5%.

Finally, let us note that the rather large values of the vertex constants C raise the question whether multiple-jet processes might not yield larger contributions to the single-particle cross section than the two-jet process described above. This self-consistency aspect of the model will be discussed further in Sec. V.

III. MODEL FOR TRIPLE-JET PRODUCTION

Figure 4 is the natural extension of Fig. 2 for the production of three large-p_T jets. In this section, the three-jet invariant cross section due to this process is considered. After deriving this result, we integrate over the momentum of one of the jets and multiply by λ^2 to obtain the two-meson invariant cross section. Thus the hard scattering eventually considered is

$$q + \bar{q} \to \text{two mesons (detected)} + \text{jet (meson quantum numbers)}. \tag{3.1}$$

Hence we expect, using (1.3),

$$E_1 E_2 \frac{d\sigma}{d^3p_1 d^3p_2} \simeq s^{-6} H(\text{dimensionless invariants}). \tag{3.2}$$

As before, it is assumed that the triggers are dominated by the single-particle modes of the jets.

However, there is less justification for the assumption in this instance. When two large-p_T particles are detected, the transverse momentum falloffs need not be as rapid as in the single-particle case, particularly for certain configurations in which increasing the momentum of one of the detected particles can be compensated by a decrease in the p_T of the undetected balancing jet. Consequently the multiparticle modes of the jets

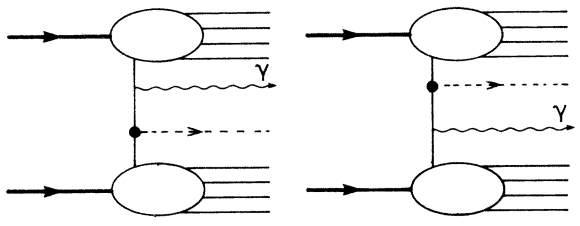

FIG. 3. Quark-fusion diagrams for direct photon production at large p_T.

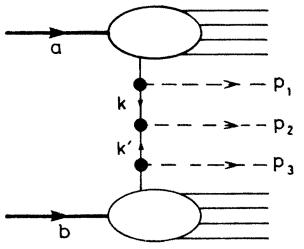

FIG. 4. Quark-fusion diagram for production of three large-p_T jets.

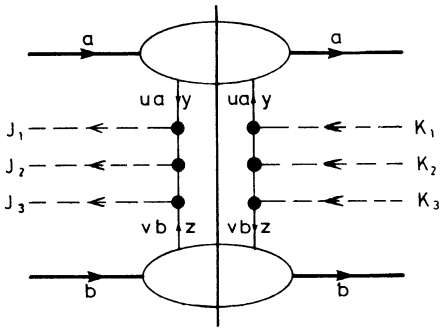

FIG. 5. General amplitude whose discontinuity contributes to our calculation of triple-jet production at large p_T.

may give a more significant contribution. In that case, (3.1) gives only a lower bound to the cross section.

The additional input necessary for the calculation of (3.1) is the form of the central jet/meson vertex of Fig. 4 which has large mass squared k^2, k'^2 in both quark legs. The Bethe-Salpeter equation approach used in Sec. II gives (see Ref. 12)

$$\gamma_5 \int_0^1 d\mu\, \eta(\mu)[\mu k^2 + (1-\mu)k'^2]^{-\gamma} \tag{3.3}$$

for the pseudoscalar-meson vertex (again keeping the γ-matrix structure simple). Taking $\gamma = \frac{1}{2}$ gives the dimensional counting result for the hard scattering and is consistent with the vertex used in Sec. II when one of k^2, k'^2 is kept fixed while the other becomes large. As before, a similar form is used for the jet vertex.

In the calculation we take $\eta(\mu)$ proportional to $[\delta(\mu-\alpha)+\delta(\mu-(1-\alpha))]$, and vary α between 0 and $\frac{1}{2}$ to examine the effect of choosing different weight functions η. (A sum of two δ functions is used so as to leave the vertex invariant under the interchange of k^2 and k'^2.) The magnitude of $\eta(\mu)$ is constrained by our requiring that $C_M\gamma_5(-k^2)^{-1/2}$ or $C_{\rm jet}(-k^2)^{-1/2}$ be obtained when k'^2 is held fixed and k^2 becomes large.

The resulting meson and jet (central) vertices used in the calculation of Fig. 4 are

$$C_M\gamma_5 Z(\alpha, k^2, k'^2),$$
$$C_{\rm jet} Z(\alpha, k^2, k'^2),$$

respectively, where

$$Z(\alpha, k^2, k'^2) = \frac{[\alpha(1-\alpha)]^{1/2}}{\sqrt{\alpha}+(1-\alpha)^{1/2}} \times\{[\alpha k^2+(1-\alpha)k'^2]^{-1/2} + (k^2 \rightarrow k'^2)\}\ , \quad 0<\alpha\leq\tfrac{1}{2}\ . \tag{3.4}$$

An important point for the calculation is that not all contributions from interference terms vanish, although the assumption of U(3) symmetry for the jet couplings still results in considerable simplification.

We use Sudakov parameters l_i, m_i to express the three jet momenta p_i of Fig. 4 partially in terms of the incoming proton momenta a, b,

$$p_i = l_i a + m_i b + p_{iT} \quad (i=1,2,3)\ , \tag{3.5}$$

where

$$a\cdot p_{iT} = b\cdot p_{iT} = 0,$$
$$p_{iT}^2 = -\vec{p}_{iT}^{\,2}\ .$$

The parameters l_i, m_i are related to $\vec{p}_{iT}, \theta_i$ by

$$\vec{p}_{iT}^{\,2} \simeq l_i m_i s\ ,$$
$$\cot\tfrac{1}{2}\theta_i \simeq \left(\frac{l_i}{m_i}\right)^{1/2} \tag{3.6}$$

(for jets with limited finite invariant mass as $p_T, \sqrt{s}$ become large together).

Figure 5 shows the general amplitude whose discontinuity contributes to the three-jet inclusive cross section in our model. In Fig. 5 (J_1, J_2, J_3) and (K_1, K_2, K_3) are permutations of (p_1, p_2, p_3). We will use J and K to label the corresponding permutations of (1, 2, 3). The six permutations of (1,2, 3) are numbered as follows:

$$\begin{aligned} &1.\ (1,2,3),\quad 2.\ (1,3,2),\quad 3.\ (2,3,1),\\ &4.\ (2,1,3),\quad 5.\ (3,1,2),\quad 6.\ (3,2,1). \end{aligned} \tag{3.7}$$

Thus the diagram corresponding to $(J, K) = (2, 6)$ is Fig. 5 with $(J_1, J_2, J_3) = (p_1, p_3, p_2)$ and $(K_1, K_2, K_3) = (p_3, p_2, p_1)$.

The term denoted by Fig. 5 can be identified with the term in the squared total amplitude for three-jet production, consisting of the product of the amplitude of Fig. 4 with permutation J of the p_i and that with permutation K, summed over the final states of the quark-proton amplitudes. Thus the cross terms correspond to Fig. 5 with $J \neq K$.

We now derive an expression for the contribution of Fig. 5 for arbitrary (J, K) in the limit as s becomes large with l_i, m_i fixed. First note that

$$\begin{aligned} J_i &= l_{J(i)} a + m_{J(i)} b + p_{J(i)T} \quad (i=1,2,3)\ ,\\ K_i &= l_{K(i)} a + m_{K(i)} b + p_{K(i)T}\ . \end{aligned} \tag{3.8}$$

Let y, z label the partons participating in the hard scattering. Let y, z carry fractions u, v of their parent protons' momenta a, b, respectively. Then the distribution functions for y, z are $F_2^y(u^{-1})/u$, $F_2^z(v^{-1})/v$, respectively, and the contribution of Fig. 5 to $E_1E_2E_3 d\sigma/d^3p_1 d^3p_2 d^3p_3$ is

$$\simeq \int_0^1 du\,dv \frac{F_2^y(u^{-1})F_2^z(v^{-1})}{uv} \frac{1}{8(2\pi)^9} \frac{|M|^2}{2uvs} (2\pi)^4 \delta^4(ua + vb - \sum p_i) \ , \tag{3.9}$$

where $|M|^2$ is that part of the squared total amplitude for

$$y + z \to \text{three jets}$$
$$(ua) \quad (vb) \quad (p_1, p_2, p_3)$$

associated with Fig. 5.

To leading order in s

$$|M|^2 \simeq C_{\text{jet}}{}^6 (um_{J(1)}s)^{-3/2} Z(\alpha, um_{J(1)}s, vl_{J(3)}s)(vl_{J(3)}s)^{-3/2}(vl_{K(3)}s)^{-3/2}$$
$$\times Z(\alpha, um_{K(1)}s, vl_{K(3)}s)(um_{K(1)}s)^{-3/2} \mathrm{Tr}[u\not{a}(u\not{a} - \not{J}_1)(\not{J}_3 - v\not{b})v\not{b}(\not{K}_3 - v\not{b})(u\not{a} - \not{K}_1)]^{\frac{1}{4}} \ ,$$

where the internal quark propagators have been included and an average has been taken over the spins of y and z. This leads to

$$|M|^2 \simeq \frac{C_{\text{jet}}{}^6 Z(\alpha, um_{J(1)}, vl_{J(3)}) Z(\alpha, um_{K(1)}, vl_{K(3)})}{4s^7(uv)^2(m_{J(1)}l_{J(3)}l_{K(3)}m_{K(1)})^{3/2}} \mathrm{Tr}(\not{a}\not{J}_1\not{J}_3\not{b}\not{K}_3\not{K}_1) \ . \tag{3.10}$$

This is a rather heuristic derivation so far. A more rigorous approach would take greater care over relating the discontinuities of the forward quark-proton amplitudes in Fig. 5 to the deep-inelastic structure functions $F_2^{y,z}(\omega)$. Such an approach is used in Ref. 9. It does not alter the results given here.

Performing the double integration in (3.9) and using the expression for $|M|^2$ in (3.10) gives

$$\delta^2(\sum \vec{p}_{iT}) C_{\text{jet}}{}^6 W_{y,z;J,K}$$

where

$$W_{y,z;J,K} = \frac{Z(\alpha, um_{J(1)}, vl_{J(3)}) Z(\alpha, um_{K(1)}, vl_{K(3)})}{(4\pi)^5 s^9 (uv)^4 (m_{J(1)}l_{J(3)}l_{K(3)}m_{K(1)})^{3/2}} F_2^y(u^{-1}) F_2^z(v^{-1}) \mathrm{Tr}(\not{a}\not{J}_1\not{J}_3\not{b}\not{K}_3\not{K}_1) \ , \tag{3.11}$$

where now $u = \sum l_i$, $v = \sum m_i$.

Summing over all contributing $q\bar{q}$ pairs (y,z) for a given permutation (J,K), and then over all (J,K), gives the three-jet cross section

$$E_1E_2E_3 \frac{d\sigma}{d^3p_1 d^3p_2 d^3p_3} \simeq \delta^2(\sum \vec{p}_{iT}) C_{\text{jet}}{}^6 W \ , \tag{3.12}$$

where W is a sum over the functions $W_{y,z;J,K}$ defined by (3.11). The δ function in (3.12) reflects the fact that in this model the (inclusive) production of three large-p_T jets is due to an (exclusive) subprocess, and the generation of large p_T is confined to this subprocess. The δ function is the leading order approximation, in the sense that, in practice, it is smeared out over a finite region due to the finite transverse momenta of y and z.

The two-meson cross section is obtained from (3.12) by integrating over one of the jet momenta and multiplying by $\lambda^2 = C_M{}^4/C_{\text{jet}}{}^4$. This gives

$$E_1E_2 \frac{d\sigma}{d^3p_1 d^3p_2} \simeq C_M{}^4 C_{\text{jet}}{}^2 \int d^4p_3 2\delta^+(l_3m_3s - \vec{p}_{3T}{}^2)\delta^2(\sum \vec{p}_{iT}) W$$
$$\simeq \lambda^{1/2}(C_M C_{\text{jet}})^3 \int_0^1 dl_3 dm_3 \delta(l_3m_3 - \tfrac{1}{4}x_{T3}^2) W \ , \tag{3.13}$$

where

$$x_{T3} = \frac{2|\vec{p}_{1T} + \vec{p}_{2T}|}{\sqrt{s}} \ .$$

From (3.11), since the trace is $O(s^3)$, it follows that (3.13) does indeed scale as (3.2).

For completeness, we give an explicit form for the expansion of the trace in (3.11). The general result is (to leading order in s)

$$\mathrm{Tr}(\not{a}\not{J}_1\not{J}_3\not{b}\not{K}_3\not{K}_1) = \tfrac{1}{2}s^3\Big[\frac{2J_1\cdot K_1}{s}\Big(\frac{4J_3\cdot K_3}{s} - l_{J(3)}m_{K(3)} - l_{K(3)}m_{J(3)}\Big) + \frac{2J_1\cdot K_3}{s}(l_{J(3)}m_{K(1)} + l_{K(1)}m_{J(3)})$$
$$+ \frac{2J_3\cdot K_1}{s}(l_{J(1)}m_{K(3)} + l_{K(3)}m_{J(1)}) - \frac{2J_3\cdot K_3}{s}(l_{J(1)}m_{K(1)} + l_{K(1)}m_{J(1)})$$
$$+ \frac{2J_1\cdot J_3}{s}(l_{K(3)}m_{K(1)} - l_{K(1)}m_{K(3)}) + \frac{2K_1\cdot K_3}{s}(l_{J(3)}m_{J(1)} - l_{J(1)}m_{J(3)})\Big] \ . \qquad (3.14)$$

For any particular choice of (J,K), some of the terms in (3.14) vanish in leading order. For example, if $J=K$ then $2J_1\cdot K_1/s$, $2J_3\cdot K_3/s = o(1)$.

IV. CALCULATION

In this section, quantitative predictions are given for $pp \to \pi\pi + X$ at high energy and for large pion transverse momenta ($p_T \gtrsim 1.5$ GeV/c). The results of Sec. III can also be applied to obtain predictions for other beams and other double-meson triggers.

We start from (3.11). The dependence of the functions $W_{y,z;J,K}$ on y and z is contained in the factor $F_2^y(u^{-1})F_2^z(v^{-1})$. These structure functions are again taken to be given by (2.6). Accordingly, when $W_{y,z;J,K}$ is summed over the contributing $q\bar{q}$ pairs (y,z), this is equivalent to replacing $F_2^y(u^{-1})F_2^z(v^{-1})$ in (3.11) by a certain linear combination of $R(u^{-1})D(v^{-1})$, $D(u^{-1})R(v^{-1})$, and $D(u^{-1})$

TABLE I. See text. Each entry gives the relevant coefficients of $R(u^{-1})D(v^{-1})$, $D(u^{-1})R(v^{-1})$, and $D(u^{-1})D(v^{-1})$ in that order. If all three coefficients are zero, the corresponding entry is left blank. In each column heading, the first pion is the one with momentum p_1 (the second having p_2). To obtain the coefficients for π^0–π^+, π^-–π^+, and π^0–π^-, note that interchanging the momenta of the two pions is equivalent to the interchanges $1 \leftrightarrow 4$, $2 \leftrightarrow 3$, and $5 \leftrightarrow 6$ in J and K, and that the coefficients for (J,K) and (K,J) are the same.

J,K	π^+–π^+	π^+–π^0	π^+–π^-	π^-–π^-	π^-–π^0	π^0–π^0
1,1		$3,\frac{3}{2},3$	6,3,6		$\frac{3}{2},\frac{3}{2},3$	$\frac{9}{4},\frac{3}{2},3$
2,2	2,2,2	$2,\frac{3}{2},2$	2,1,2	1,1,2	$1,\frac{3}{2},2$	$\frac{3}{2},\frac{3}{2},2$
3,3	2,2,2	$\frac{3}{2},2,2$	1,2,2	1,1,2	$\frac{3}{2},1,2$	$\frac{3}{2},\frac{3}{2},2$
4,4		$3,\frac{3}{2},3$	3,3,6		$\frac{3}{2},\frac{3}{2},3$	$\frac{9}{4},\frac{3}{2},3$
5,5		$\frac{3}{2},3,3$	3,3,6		$\frac{3}{2},\frac{3}{2},3$	$\frac{3}{2},\frac{9}{4},3$
6,6		$\frac{3}{2},3,3$	3,6,6		$\frac{3}{2},\frac{3}{2},3$	$\frac{3}{2},\frac{9}{4},3$
2,1		$0,\frac{1}{2},0$			$0,-\frac{1}{2},0$	
3,1						
4,1		$-3,-\frac{3}{2},-3$			$-\frac{3}{2},-\frac{3}{2},-3$	$\frac{9}{4},\frac{3}{2},3$
5,1			2,1,2			$\frac{3}{2},\frac{3}{2},2$
6,1			2,2,2			$\frac{3}{2},\frac{3}{2},2$
3,2	2,2,2			1,1,2		$\frac{3}{2},\frac{3}{2},2$
4,2		$0,-\frac{1}{2},0$			$0,\frac{1}{2},0$	
5,2						
6,2						
4,3						
5,3		$-\frac{1}{2},0,0$			$\frac{1}{2},0,0$	
6,3		$\frac{1}{2},0,0$			$-\frac{1}{2},0,0$	
5,4			1,1,2			$\frac{3}{2},\frac{3}{2},2$
6,4			1,2,2			$\frac{3}{2},\frac{3}{2},2$
6,5		$-\frac{3}{2},-3,-3$			$-\frac{3}{2},-\frac{3}{2},-3$	$\frac{3}{2},\frac{9}{4},3$

$D(v^{-1})$. There is no $R(u^{-1})R(v^{-1})$ term because of the absence of valence antiquarks in the proton.

The coefficients in this linear combination depend on the detected mesons and on (J,K). As remarked earlier, certain simplifications occur because the final states in the balancing jet are taken to form nonets with U(3)-symmetric couplings to the quarks. Table I lists these coefficients for the six two-pion charge combinations and the 21 different (J,K). [It is easy to show that the cross section contributions from (J,K) and (K,J) are identical. Thus of the 36 diagrams of Fig. 5, no more than 21 give independent contributions.]

The blank entries in Table I denote diagrams of Fig. 5 which, from considerations of quantum number flow and, in particular, the U(3) jet couplings, can be shown to give no net contribution to the relevant two-pion combination. The fractional values in Table I arise from the $1/\sqrt{2}$ of the π^0 quark wave function.

For the calculation, we take the parameters α and λ to have the values

$$\alpha = 0.5, \quad \lambda = 5\% . \tag{4.1}$$

The variation in our results for different values of α has been investigated and found to be relatively small. $\alpha = 0.5$ gives the maximum value of $|Z(\alpha, k^2, k'^2)|$ for fixed k^2, k'^2. However, in going from $\alpha = 0.5$ to $\alpha = 0.1$, our predictions are decreased (roughly uniformly) only by about a factor of 2. A similar decrease is obtained in taking $\lambda = 1\%$ instead of 5%, since (3.13) only has a square root dependence on λ.

The main normalization constant $(C_M C_{\rm jet})^{1/2}$ is again taken equal to 14 GeV, in accordance with the fit to data described in Sec. II.

From the above, the function W of (3.12) can be obtained and integrated, as in (3.13), to give the two-pion invariant cross section. In actual practice, numerical integration using Gaussian quadrature was applied to (3.13) in the form

$$E_1E_2\frac{d\sigma}{d^3p_1 d^3p_2} \simeq \lambda^{1/2}(C_M C_{\rm jet})^3\left(\int_{(1/2)x_{T3}}^1 \frac{dl_3}{l_3} W\Big|_{m_3 = x_{T3}^2/4l_3} + \int_{(1/2)x_{T3}}^1 \frac{dm_3}{m_3} W\Big|_{l_3 = x_{T3}^2/4m_3}\right) . \tag{4.2}$$

This splitting of the integral gave better convergence properties.

In calculating specific large-$\vec{p}_{1T}, \vec{p}_{2T}$ cross sections, it should be remembered that the results will not in general be valid unless $|\vec{p}_{1T}+\vec{p}_{2T}|$, the balancing transverse momentum of the jet, is also large. This imposes a strong restriction on practical calculations for $\phi \simeq 180°$.

All the results presented below are calculated for the ISR energy point $\sqrt{s} = 52.7$ GeV. Predictions at other energies can be obtained by scaling according to (3.2) (keeping x_{T1}, x_{T2} fixed rather than $|\vec{p}_{1T}|, |\vec{p}_{2T}|$, etc.).

Table II gives the model predictions of the invariant cross sections for producing a large-p_T π^+ (particle 1) and a large-p_T π^- (particle 2). Both pions have zero center-of-mass rapidity y. The cross sections are given for $x_{T2} = 0.06, 0.08, 0.1, 0.12$ ($p_T \simeq 1.58$, 2.11, 2.64, 3.16 GeV/c, respectively) and azimuthal separations $\phi = 0°$, 90°, 120°; $x_{T1} = 0.1$ throughout. Also shown are the relative multiplicities of the other two-pion combinations at each of these values of (x_{T2}, ϕ). Table III gives the same results for $y_1 = 0$, $y_2 \simeq 1.6$. ($y_2 = \ln 5 \simeq 1.6$ corresponds to the convenient choice $l_2 = \frac{5}{2}x_{T2}, m_2 = \frac{1}{10}x_{T2}$.)

Obtaining results at $\phi = 180°$ is complicated by the restriction to large $|\vec{p}_{1T}+\vec{p}_{2T}|$ noted above. A final row in each of Tables II and III gives predictions of the model for $x_{T1} = 0.14$, $x_{T2} = 0.07$ ($p_{T1} \simeq 3.69$ GeV/c, $p_{T2} = |\vec{p}_{1T}+\vec{p}_{2T}| \simeq 1.84$ GeV/c) at $\phi = 180°$.

The zeros among the $\phi = 0°$ entries of Table II represent the vanishing of the predicted cross section to leading order in s. For $\pi^+ - \pi^+$ and $\pi^- - \pi^-$, this is because all the contributing diagrams contain the factor $2p_1 \cdot p_2/s$ which is $o(1)$ at $\phi = 0°$. The other zeros in the $\phi = 0°$, $x_{T2} = 0.1$ row result from destructive interference.

The entries of Tables II and III satisfy the identity

$$\sum_{c=+,0,-} [d\sigma(\pi^+\pi^c) + d\sigma(\pi^-\pi^c) - 2d\sigma(\pi^0\pi^c)] = 0 . \tag{4.3}$$

This is a special case of

$$d\sigma(\pi^+) + d\sigma(\pi^-) = 2d\sigma(\pi^0) . \tag{4.4}$$

Equations (4.3) and (4.4) are isospin relations which hold in models, such as quark fusion, in which the production mechanisms are proton $+I$-spin singlet $\to \pi\pi + X, \pi + X$, respectively.[18] The isosinglet for the case of quark fusion is the quark sea of one of the protons.

The results set out in Tables II and III have certain interesting features.

Owing to the variety in contributing processes and the existence of large cross terms, the relative multiplicities of the two-pion charge states cover a wide range and they have significant dependence on y_2, ϕ, and x_{T2}.

TABLE II. Predictions of the three-jet model of the text for various two-pion inclusive cross sections at large p_T in pp interactions. $x_T = 2p_T/\sqrt{s}$, ϕ is azimuthal separation of the two pions, y is the center-of-mass rapidity. The subscripts 1 and 2 denote the first and second pions in each column heading, respectively. $\sqrt{s} = 52.7$ GeV. Predictions for other energies can be obtained by scaling according to (3.2). At $\sqrt{s} = 52.7$ GeV, $x_T = 0.06$, 0.07, 0.08, 0.1, 0.12, and 0.14 correspond to $p_T \simeq 1.58$, 1.84, 2.11, 2.64, 3.16, and 3.69 GeV/c, respectively.

$y_1 = y_2 = 0$			$E_1E_2\frac{d\sigma}{d^3p_1 d^3p_2}(\pi^+\pi^-)$	Other $\pi\pi$ combinations relative to $\pi^+\pi^-$							
ϕ	x_{T1}	x_{T2}	(mb GeV$^{-4}c^6$)	$\pi^+\pi^0$	$\pi^-\pi^0$	$\pi^+\pi^+$	$\pi^-\pi^-$	$\pi^0\pi^0$	$\pi^-\pi^+$	$\pi^0\pi^+$	$\pi^0\pi^-$
0°	0.1	0.06	6.7×10^{-9}	0.03	0.02	0	0	1.02	1.08	0.03	0.02
		0.08	1.3×10^{-9}	0.005	0.004	0	0	1.01	1.03	0.005	0.004
		0.1	3.1×10^{-10}	0	0	0	0	1	1	0	0
		0.12	8.4×10^{-11}	0.003	0.002	0	0	0.98	0.97	0.003	0.002
90°	0.1	0.06	5.0×10^{-8}	0.34	0.30	0.04	0.02	0.74	1.06	0.34	0.29
		0.08	1.2×10^{-8}	0.31	0.28	0.04	0.02	0.75	1.02	0.32	0.28
		0.1	3.0×10^{-9}	0.30	0.27	0.05	0.03	0.75	1	0.30	0.27
		0.12	8.3×10^{-10}	0.29	0.26	0.05	0.03	0.76	0.98	0.29	0.26
120°	0.1	0.06	2.6×10^{-7}	0.58	0.48	0.06	0.03	0.53	1.04	0.58	0.49
		0.08	8.0×10^{-8}	0.56	0.46	0.05	0.03	0.54	1.02	0.55	0.46
		0.1	2.2×10^{-8}	0.53	0.45	0.05	0.03	0.55	1	0.53	0.45
		0.12	5.8×10^{-9}	0.52	0.44	0.06	0.03	0.56	0.99	0.52	0.44
180°	0.14	0.07	7.6×10^{-8}	1.06	0.82	0.06	0.03	0.10	0.99	1.02	0.86

The cross sections, as a whole, decrease with x_{T2} and increase with ϕ as expected (increasing ϕ decreases the total transverse momentum generated in the hard scattering). Most, though not all, cross sections are higher at $y_2 \simeq 1.6$ than at $y_2 = 0$. The x_T, ϕ, and y_2 dependences of the $\pi^+ - \pi^-$ cross section are looked at in more detail below.

Table IV gives the results expected on the basis of an independent-production picture, where

$$E_1E_2\frac{d\sigma}{d^3p_1 d^3p_2} = \frac{1}{\sigma_{\text{inelastic}}} E_1\frac{d\sigma}{d^3p_1} E_2\frac{d\sigma}{d^3p_2} \quad . \tag{4.5}$$

The single-particle cross sections for calculating (4.5) are taken from the π^0 data of Ref. 8 and the π^+, π^- data of Ref. 6. Table IV gives only the dependence on x_T, since there is obviously no ϕ dependence in (4.5) and the variation of the single-

TABLE III. See caption to Table II.

$y_1 = 0, y_2 \simeq 1.6$			$E_1E_2\frac{d\sigma}{d^3p_1 d^3p_2}(\pi^+\pi^-)$	Other $\pi\pi$ combinations relative to $\pi^+\pi^-$							
ϕ	x_{T1}	x_{T2}	(mb GeV$^{-4}c^6$)	$\pi^+\pi^0$	$\pi^-\pi^0$	$\pi^+\pi^+$	$\pi^-\pi^-$	$\pi^0\pi^0$	$\pi^-\pi^+$	$\pi^0\pi^+$	$\pi^0\pi^-$
0°	0.1	0.06	1.5×10^{-8}	0.67	0.54	0.26	0.14	0.77	1.35	0.68	0.53
		0.08	1.8×10^{-9}	0.70	0.58	0.34	0.18	0.82	1.40	0.73	0.54
		0.1	2.9×10^{-10}	0.72	0.63	0.42	0.22	0.88	1.49	0.80	0.55
		0.12	5.1×10^{-11}	0.76	0.69	0.50	0.25	0.96	1.61	0.89	0.56
90°	0.1	0.06	1.1×10^{-7}	0.73	0.56	0.22	0.12	0.70	1.34	0.73	0.55
		0.08	1.6×10^{-8}	0.75	0.59	0.28	0.15	0.74	1.39	0.78	0.56
		0.1	2.8×10^{-9}	0.78	0.62	0.35	0.18	0.79	1.45	0.83	0.57
		0.12	5.1×10^{-10}	0.82	0.67	0.43	0.22	0.85	1.55	0.91	0.58
120°	0.1	0.06	5.9×10^{-7}	0.74	0.55	0.14	0.07	0.64	1.35	0.74	0.55
		0.08	1.1×10^{-7}	0.75	0.56	0.16	0.09	0.66	1.38	0.76	0.55
		0.1	2.0×10^{-8}	0.77	0.58	0.21	0.11	0.69	1.43	0.80	0.55
		0.12	3.5×10^{-9}	0.80	0.61	0.26	0.14	0.74	1.50	0.86	0.56
180°	0.14	0.07	3.0×10^{-7}	0.76	0.55	0.04	0.02	0.56	1.37	0.75	0.56

TABLE IV. "Independent production" results (see text) for a two-pion invariant cross section at $\sqrt{s} = 52.7$ GeV. The dependence on the particular $(\pi\pi)$ charge combination and (moderate values of) y_1, y_2 is small and comparable to the uncertainties in the large-p_T single-pion data from which the entries are calculated.

x_{T1}	x_{T2}	$E_1E_2\frac{d\sigma}{d^3p_1 d^3p_2}(\pi\pi)$ (mb GeV^{-4} c^6)
0.1	0.06	9.0×10^{-7}
	0.08	1.3×10^{-7}
	0.1	2.4×10^{-8}
	0.12	3.9×10^{-9}
0.14	0.07	1.2×10^{-8}

pion cross sections with charge and rapidity (up to $y \simeq 1.5$) is fairly small. Comparing Table IV with Tables II and III shows that if there is such independent production of the two large-p_T pions, the resulting cross sections are in most cases comparable with, or exceed, those due to the

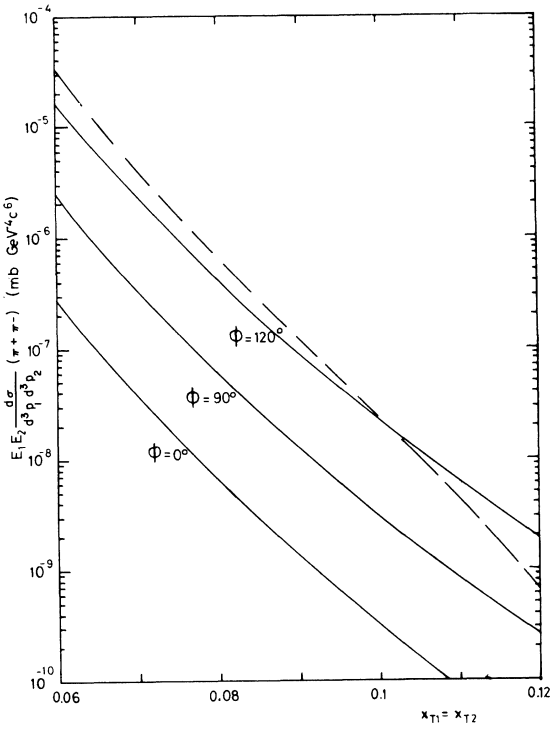

FIG. 6. Triple-jet prediction for the π^+-π^- invariant cross section, plotted as a function of $x_{T1}=x_{T2}$ for $\phi=0°$, 90°, and 120°. $y_1=y_2=0$. The absolute normalization corresponds to $\sqrt{s}=52.7$ GeV. The dashed line is the independent production result at this energy. Since the two processes scale differently, the dashed line will fall faster than the solid lines as the energy is increased.

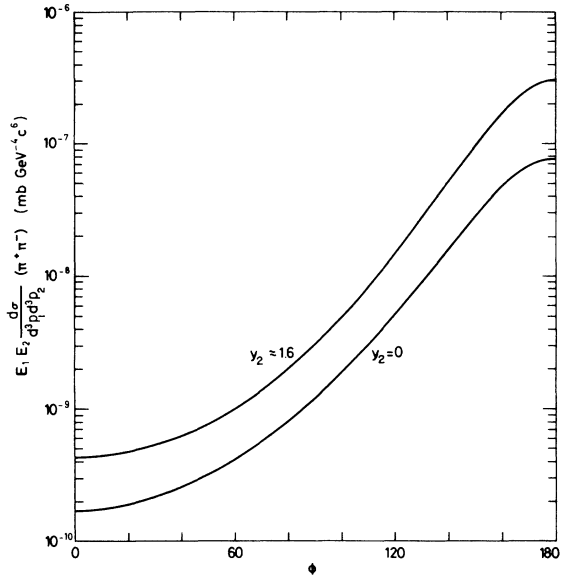

FIG. 7. Triple-jet prediction for the π^+-π^- invariant cross section, plotted as a function of the azimuthal separation ϕ for $y_2=0$ and $\simeq 1.6$. $x_{T1}=0.14$, $x_{T2}=0.07$. $y_1=0$. Subscripts 1, 2 denote the π^+, π^- respectively. The absolute normalization corresponds to $\sqrt{s}=52.7$ GeV. The corresponding independent-production result at this energy is 1.2×10^{-8} mb GeV^{-4} c^6.

three-jet mechanism considered here. However, at higher energies (with x_{T1}, x_{T2}, etc. fixed) the three-jet contribution is expected to be the more important because of the scaling behavior of (4.5) implied by (2.2). This is in fact already the case for our results at $\phi = 180°$. These points are discussed further below.

The x_T, ϕ, and y_2 variations noted in Tables II and III are examined further for the case of the π^+-π^- cross section in Figs. 6, 7 and 8. Figure 6 shows the dependence on $x_{T1}=x_{T2}$ for $\phi=0°$, 90°, and 120° with $y_2=0$. The independent production result is also displayed. Figure 7 gives the variation with ϕ for $y_2=0$ and $y_2\simeq1.6$. Figure 8 gives the variation with y_2 for $\phi=0°$, 90°, and 180°. All these figures have $y_1=0$. Figures 7 and 8 have $x_{T1}=0.14$, $x_{T2}=0.07$ so as to allow inclusion of $\phi=180°$ in the plots. Subscripts 1, 2 denote the π^+, π^- respectively. One interesting conclusion to be drawn from Tables II, III and Figs. 7, 8 is that, to increase (three-jet) event rates, the detector for the pion with smaller p_T should be set away from $\theta=90°$.

Our predictions can be compared with data in two regions. The CERN-Columbia-Rockefeller-Saclay collaboration (CCRS) at CERN ISR have performed an experiment[8] on large-p_T two-particle correlations, with momentum measurement, at $\phi\simeq0°$ and

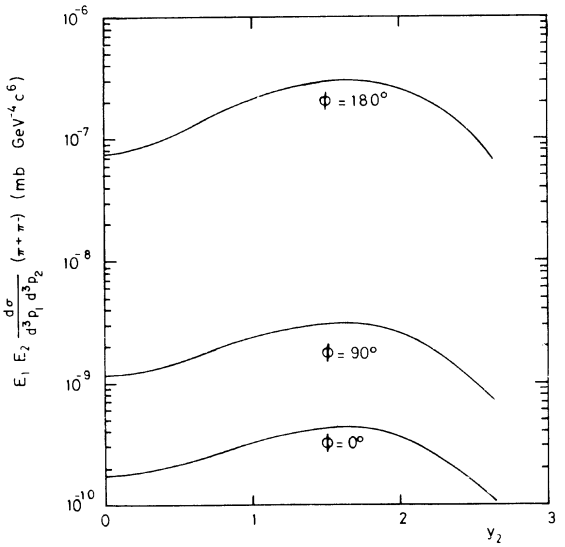

FIG. 8. Triple-jet prediction for the π^+-π^- invariant cross section, plotted as a function of the π^- rapidity y_2 for $\phi = 0°$, 90°, and 180°. $x_{T1} = 0.14$, $x_{T2} = 0.07$. $y_1 = 0$. The absolute normalization corresponds to $\sqrt{s} = 52.7$ GeV. The corresponding independent production result at this energy is 1.2×10^{-8} mb GeV^{-4} c^6.

$\phi \simeq 180°$. (Note, however, that there is some uncertainty in a direct comparison with our results as CCRS measure a partially-integrated two-particle cross-section). Since, in our picture, the correlations at $\phi \simeq 0°$, 180° are largely due to the two-jet process of Sec. II (see for example Ref. 13), we require the three-jet results to fall below these data. At $\phi \simeq 0°$, our predictions are orders of magnitude lower than the data. At $\phi \simeq 180°$, the prediction of Table II, although higher than independent production, appears to be below the data by a factor of about 5, possibly more.

Finally in this section, let us consider some aspects of the dependence of our results on our particular assumptions:

We note that the simple parton distributions of (2.6) are probably inaccurate at small ω (and the sea distribution is only poorly determined experimentally in any case). This should not have too much effect on our results, which are at low x_T, with the possible exception of those at large rapidity.

If, instead of quark fusion, we had started from a meson-bremsstrahlung process[22] for large-p_T single-meson production, and generalized *that* (to $qM \to MMq$ via t-channel quark exchange), then because the relevant vertices would have a similar form and size,[14] our intuitive expectation is that the y, ϕ, and x_T distributions would be similar in shape and roughly of the same order of magnitude. However, the relative magnitudes of the different $\pi\pi$ combinations could be completely different. (The latter also depend somewhat on the assumption that only the single-particle modes of the jets contribute significantly to the large-p_T triggers.) Also, we would not be confident of any such similarity in the case of an extended qq-scattering model.

V. DISCUSSION

Firstly let us consider the question of the contribution of the three-jet process to single-meson cross sections at large p_T. This is rather difficult to assess because, in integrating over $\vec{p}_2$ in (3.13), one is confined to regions of phase space in which $|\vec{p}_{2T}|$ and $|\vec{p}_{1T} + \vec{p}_{2T}|$ are both sufficiently large so that not only is a three-jet description appropriate (one of the jets of Fig. 4 cannot be just simply absorbed into the low-p_T quark-hadron amplitudes of Fig. 2), but also so that the restriction of our calculation to the leading order term is valid.

Most of the three-jet contribution to the single-particle cross section comes from near the edges of these regions, and, since the boundaries are ill defined, the difficulty is a real one. As can be seen from Fig. 7, the important contribution to the single-particle cross section comes from nearly coplanar three-jet processes, and consequently the situation is rather similar to that encountered in calculating the two-meson cross section at $\phi \simeq 180°$. It might be thought that the apparently small contribution of the three-jet process to the two-particle correlation data of CCRS at $\phi \simeq 180°$ is encouraging. However, the contribution of this process to the single-particle cross section comes from integrating over

$$\sum_M E_1 E_2 \frac{d\sigma}{d^3p_1 d^3p_2}(\pi_1, \text{ jet with } "M" \text{ quantum numbers})$$

rather than

$$\sum_M E_1 E_2 \frac{d\sigma}{d^3p_1 d^3p_2}(\pi_1, M) .$$

The former exceeds the latter in our picture by a factor $\lambda^{-1} = 20$.

For the reasons outlined above, it is difficult to give a definite result. However, after examining this problem in some detail, we find it hard to avoid the conclusion that, in the model, the three-jet mechanism is likely to contribute significantly to single-particle cross sections, at least for certain values of p_T.

Some remarks must be made concerning the normalization of our results. As noted earlier, the predictions for the two-pion cross sections can reasonably be reduced by two (independent) factors of two in overall normalization (by taking

$\lambda = 1\%$, $\alpha = 0.1$). However, in the opposite direction, there may well be a significant additional contribution to these results from the multiparticle modes of the jets, since the trigger bias may not as strongly select the single-particle modes as is the (assumed) case for large-p_T single-meson production. This effect arises from the possibility of less rapid p_T falloffs and may be especially important at $\phi \simeq 180°$ for the pion with the smaller p_T.

Also, since our value for $(C_M C_{\text{jet}})$ comes from a fit to large-p_T single-particle data, it should be noted that such data from different experiments have absolute normalization discrepancies of about a factor of 2. Our fit further assumes, of course, that (two-jet) quark fusion *is* the dominant process for this data (cf. final paragraph of Sec. IV).

Finally, one should note the enhancement which would result from color, discussed at the beginning of Sec. II.

Turning to the relevance of our results for future experiments, we note the following. If there is independent production of two large-p_T pions at the level given by (4.5), then the three-jet mechanism for this process will be hard to detect above this background at present energies for ϕ well away from 180°. As ϕ approaches 180°, the three-jet prediction becomes larger than independent production. However, in this region a contribution from two-jet processes is encountered which arises from the tail in the particle distributions of the jets transverse to the jet axis. For these reasons it may be difficult to obtain clear experimental evidence for the three-jet model of this paper from two-pion cross sections.

On the other hand, since the three-jet cross sections are largest when the jets are coplanar, perhaps it is possible to observe all three jets experimentally by looking for this configuration, i.e., by triggering on a particle with $p_T = X$ and looking on the opposite side of the beam(s) for two particles with $p_T \gtrsim \frac{1}{3}X$ (say) and having a large rapidity gap (so as to avoid the two-jet processes).[19] This may be feasible with the present experimental facilities at the CERN Split-Field Magnet.

This conclusion is at variance with our initial motivation that, by looking at $\phi = 90°$, say, multiple-jet processes could be observed independently of the two-jet process. In our model, $\phi = 90°$ may only produce interesting results if independent production is at a rather lower level than that given by (4.5).

However, as discussed in the Introduction, this may well be the case, and our preceding remarks may be too pessimistic, in which case it would appear that many of our predictions for noncoplanar $(\pi\pi)$ combinations are indeed experimentally accessible, and data on their relative multiplicities and variations with ϕ, y, and x_T could provide interesting tests for the model presented here.

Moreover, even a negative result at $\phi = 90°$ (e.g. independent production obscures more interesting dynamics) is not entirely without interest as it is not expected in all models. For example, in massive electrodynamics (although not in ϕ^3) a large-p_T trigger is expected to be accompanied by other large-p_T particles emitted in random directions.[20]

ACKNOWLEDGMENTS

I am grateful to Professor J. C. Polkinghorne and Dr. P. V. Landshoff for their advice and encouragement. I have also had useful discussions with C. O. Escobar and Dr. U. Sukhatme. I acknowledge financial support from the Science Research Council and Churchill College.

---

*Present address: CERN, Geneva, Switzerland.

[1]L. Di Lella, in *Proceedings of the 1975 International Symposium on Lepton and Photon Interactions at High Energies, Stanford, California*, edited by W. T. Kirk (SLAC, Stanford, 1976); P. Darriulat, in *High Energy Physics*, Proceedings of the European Physical Society International Conference, Palermo, 1975, edited by A. Zichichi (Editrice Compositori, Bologna, 1976). See also, for example, Ref. 13.

[2]D. Sivers, S. J. Brodsky, and R. Blankenbecler, Phys. Rep. 23C, 1 (1976).

[3]S. D. Ellis, in *Proceedings of the XVII International Conference on High Energy Physics, London, 1974*, edited by J. R. Smith (Rutherford Laboratory, Chilton, Didcot, Berkshire, England, 1974), p. V-23; P. V. Landshoff, *ibid.*, p. V-57.

[4]V. A. Matveev, R. M. Muradyan, and A. N. Tavkhelidze, Lett. Nuovo Cimento 7, 719 (1973).

[5]S. J. Brodsky and G. R. Farrar, Phys. Rev. Lett. 31, 1153 (1973); Phys. Rev. D 11, 1309 (1975).

[6]B. Alper *et al.*, Nucl. Phys. B100, 237 (1975).

[7]D. Antreasyan *et al.*, Phys. Rev. Lett. 38, 112 (1977); 38, 115 (1977).

[8]F. W. Büsser *et al.*, Nucl. Phys. B106, 1 (1976).

[9]P. V. Landshoff and J. C. Polkinghorne, Phys. Rev. D 8, 4157 (1973); 10, 891 (1974).

[10]B. L. Combridge, Phys. Lett. 62B, 222 (1976).

[11]C. O. Escobar, Phys. Rev. D 15, 355 (1977).

[12]P. V. Landshoff and J. C. Polkinghorne, Phys. Rev. D 8, 927 (1973).

[13]S. D. Ellis, M. Jacob, and P. V. Landshoff, Nucl. Phys. B108, 93 (1976).

[14]B. L. Combridge, Phys. Rev. D 10, 3849 (1974).

[15]G. Donaldson *et al.*, Phys. Rev. Lett. 36, 1110 (1976).

[16]C. O. Escobar, Nucl. Phys. B98, 173 (1975).

[17]P. Darriulat *et al.*, Nucl. Phys. B110, 365 (1976).

[18]A. J. Macfarlane, Phys. Rev. D 6, 326 (1972) and references cited therein.

[19]A different parton mechanism in which approximately coplanar multiple-jet events are produced is given by P. V. Landshoff, J. C. Polkinghorne, and D. M. Scott, Phys. Rev. D 12, 3738 (1975).

[20]I. G. Halliday, J. Huskins, and C. T. Sachrajda, Nucl. Phys. B87, 93 (1975).

[21]There are some intriguing possibilities if this condition on H_1 is not met, and if as is quite possible, the single-particle cross section should be obtained by integrating over a fixed region of $\{\tilde{q}_{k\,T}, x_{Fk}\}$ rather than $\{q_i \cdot q_j/s\}$. For example, consider $E_1E_2 d\sigma/d^3p_1 d^3p_2 \sim p_{T1}^{-N} p_{T2}^{-N}$ and $(p_{T1}^2 + p_{T\,2}^2)^{-N}$, which have the same scaling behavior for the two-particle cross section, but which give completely different scaling behaviors for $E_1 d\sigma/d^3p_1$ after integrating p_{T2} over $p_{T2} > 1$ GeV/c (say). From a quick calculation it seems that, when treated in this way, the contribution of the three-jet model, considered in Sec III, to the large-p_T single-particle yield scales as (1.2) with $N=4$ (instead of 5), the same as for the two jet process. These possibilities and their consequences are under further consideration.

[22]R. Blankenbecler, S. J. Brodsky, and J. F. Gunion, Phys. Lett. 42B, 461 (1972).

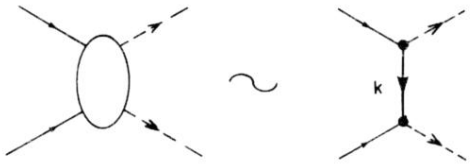

FIG. 1. Single-quark exchange approximation for the high-energy fixed-angle scattering $q+\bar{q}\rightarrow$ two jets (with meson quantum numbers).

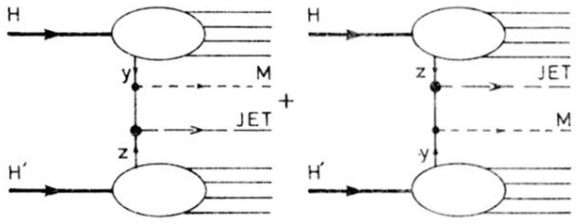

FIG. 2. (Two-jet) quark-fusion diagrams for $H+H'\to M+X$ at large p_T.

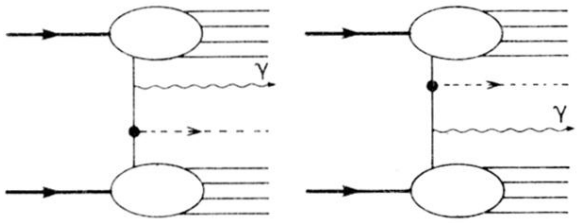

FIG. 3. Quark-fusion diagrams for direct photon production at large p_T.

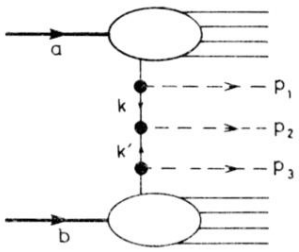

FIG. 4. Quark-fusion diagram for production of three large-p_T jets.

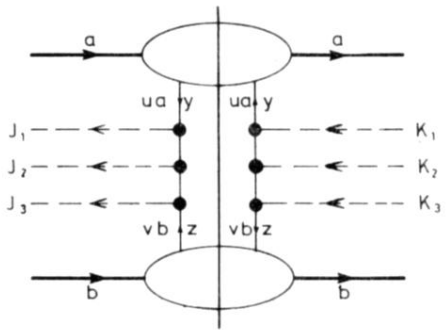

FIG. 5. General amplitude whose discontinuity contributes to our calculation of triple-jet production at large p_T.

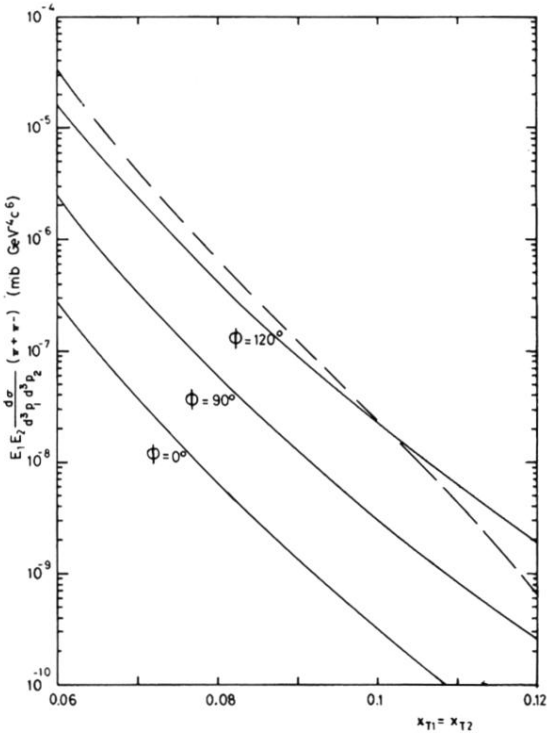

FIG. 6. Triple-jet prediction for the $\pi^+-\pi^-$ invariant cross section, plotted as a function of $x_{T1}=x_{T2}$ for $\phi=0°$, 90°, and 120°. $y_1=y_2=0$. The absolute normalization corresponds to $\sqrt{s}=52.7$ GeV. The dashed line is the independent production result at this energy. Since the two processes scale differently, the dashed line will fall faster than the solid lines as the energy is increased.

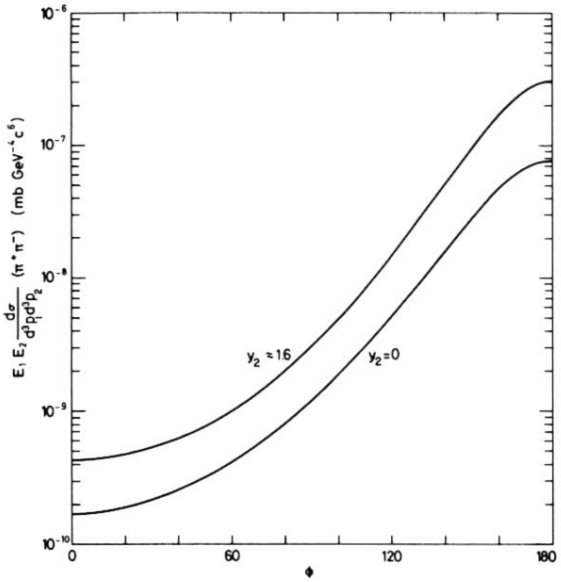

FIG. 7. Triple-jet prediction for the π^+-π^- invariant cross section, plotted as a function of the azimuthal separation ϕ for $y_2 = 0$ and $\simeq 1.6$. $x_{T1} = 0.14$, $x_{T2} = 0.07$. $y_1 = 0$. Subscripts 1, 2 denote the π^+, π^- respectively. The absolute normalization corresponds to $\sqrt{s} = 52.7$ GeV. The corresponding independent-production result at this energy is 1.2×10^{-8} mb GeV^{-4} c^6.

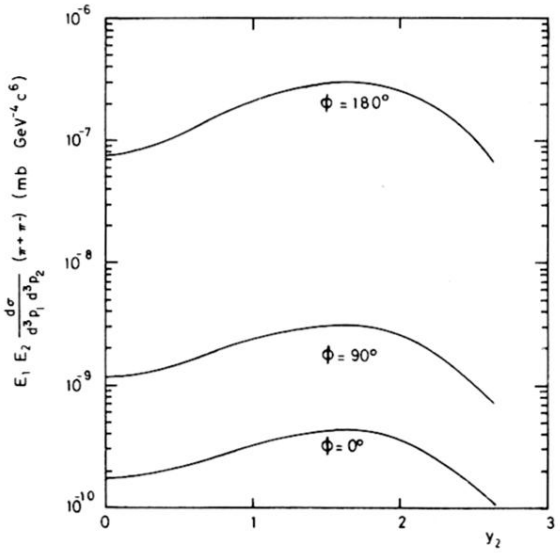

FIG. 8. Triple-jet prediction for the π^+-π^- invariant cross section, plotted as a function of the π^- rapidity y_2 for $\phi = 0°$, 90°, and 180°. $x_{T1} = 0.14$, $x_{T2} = 0.07$. $y_1 = 0$. The absolute normalization corresponds to $\sqrt{s} = 52.7$ GeV. The corresponding independent production result at this energy is 1.2×10^{-8} mb GeV^{-4} c^6.